Chemical Engineering Journal 535 (2026) 175331

Contents lists available at ScienceDirect

Chemical Engineering Journal

journal homepage: www.elsevier.com/locate/cej

Direct valorisation of bio-glycerol to acrylic acid: Experimental comparison of membrane and conventional reactors

Prashant Pawanipagar [a,*], Yash Bansod [a], Umar Abubakar [a], Hassan Alhassawi [a], Min Hu [a], Christopher De leeuwe [a], Kamran Ghasemzadeh [a,b,**], Carmine D'Agostino [a,c,**], Vincenzo Spallina [a,*]

[a] Department of Chemical Engineering, University of Manchester, Manchester, M13 9PL, UK
[b] Department of Chemical Engineering, University of Edinburgh, EH9 3JW, UK
[c] Dipartimento di Ingegneria Civile, Chimica, Ambientale e dei Materiali (DICAM), Alma Mater Studiorum – Università di Bologna, Via Terracini, 28, 40131, Bologna, Italy

ARTICLE INFO

Keywords:
Glycerol valorisation
Acrylic acid
Membrane reactor
Acrolein
Reactor testing

ABSTRACT

This study demonstrates the proof-of-principle of using a membrane reactor to enhance acrylic acid production via oxidative dehydration of glycerol. The performance of the membrane reactor was compared with that of a conventional packed-bed reactor in terms of key reaction parameters. The dehydration reaction was carried out over the HZSM-5 (SAR-200) catalyst, followed by oxidation over the Ortho-MoVO catalyst. A design of experiments and optimisation strategy was applied to maximise acrylic acid selectivity by varying temperature, oxygen-to-glycerol molar ratio, gas hourly space velocity (GSHV), and feed-to-membrane ratio. Testing was carried out using up to 30 g of catalysts (diluted with an additional 120 g of solid inert). The membrane reactor outperforms the conventional packed-bed reactor, achieving a maximum acrylic acid selectivity of 58.7% under optimised conditions (280 °C, 1935 h^{-1} GHSV, 14:1 oxygen-to-glycerol ratio, and 50:50 feed-to-membrane ratio). The superior performance of the membrane reactor is attributed to controlled oxygen distribution via the membrane, which locally maintains a lower oxygen partial pressure, in line with first-order kinetics, resulting in improved net acrylic acid selectivity, with an increase of 10% compared to a packed-bed reactor. The major by-products are acetic acid, formic acid and CO_x. Overall, this study demonstrates the potential of the intensified membrane reactor for manufacturing of value-added chemicals and its applicability to future industrial processes.

1. Introduction

Growing environmental challenges from industrial activity and fossil fuel dependence highlight the urgent need to develop sustainable chemicals from renewable resources. Biomass has therefore gained attention as an alternative energy source [1]. Biodiesel, a renewable fuel derived from biomass, has emerged as a substitute for fossil fuels, reducing environmental impacts while supporting the energy transition [2,3]. Over the past two decades, global biodiesel production has increased sharply, creating a surplus of glycerol as a by-product. This abundant and low-cost feedstock presents an opportunity for valorisation into value-added products such as lactic acid, acetic acid, acrylic acid, and solketal [4,5]. Among these, acrylic acid is particularly significant, with major applications in superabsorbent polymers (≈50% of global demand), coatings, adhesives, specialty esters, biomedical hydrogels, and water treatment systems [6,7].

Currently, acrylic acid is produced from propylene (derived from fossil fuel) via a two-step catalytic oxidation process over metal oxide catalysts, with acrolein as the key intermediate [8]. A renewable alternative, the glycerol-to-acrylic acid (GTA) route, also proceeds through acrolein as a common intermediate and involves two sequential steps: (i) dehydration of glycerol to acrolein over acid sites, e.g., zeolite HZSM-5, followed by (ii) oxidation of acrolein to acrylic acid using metal oxides, such as MoVO catalysts [9,10]. A single-reactor configuration with a

* Corresponding authors.
** Corresponding authors at: Department of Chemical Engineering, University of Manchester, Manchester, M13 9PL, UK.
E-mail addresses: prashant.pawanipagar@manchester.ac.uk (P. Pawanipagar), kghasemz@ed.ac.uk (K. Ghasemzadeh), carmine.dagostino@manchester.ac.uk (C. D'Agostino), vincenzo.spallina@manchester.ac.uk (V. Spallina).

https://doi.org/10.1016/j.cej.2026.175331
Received 8 December 2025; Received in revised form 20 February 2026; Accepted 16 March 2026
Available online 19 March 2026

combined catalyst system could be advantageous (cost benefit, increased productivity), provided that complete glycerol conversion with high acrolein selectivity in the dehydration step prevents glycerol oxidation in the second bed, thereby maximising acrylic acid selectivity [11,12]. The GTA reaction is shown below.

$$C_3H_8O_3 + \frac{1}{2}O_2 \rightarrow C_3H_4O_2 + 2H_2O \qquad \Delta H^0 = -386.5 \frac{kJ}{mol_{C_3H_8O_3}} \qquad (1)$$

Glycerol dehydration over HZSM-5 catalyst forms intermediates such as acetol, acetone, acetaldehyde, acrolein, propanal, hydroxyacetone, and acetic acid via cracking, and C—O bond rearrangements [13]. Recent studies have shown that the silica-to-alumina ratio (SAR) of HZSM-5 strongly governs its acid–base properties and, consequently, product distribution, with a SAR of 200 providing optimal acidity to maximise acrolein formation while suppressing undesired by-products [9]. However, despite its effectiveness, the use of HZSM-5 introduces a critical challenge: coke formation, a primary cause of zeolite deactivation, arises due to incomplete conversion of hydrocarbon intermediates formed during reactions such as dehydrogenation and cracking [14]. The microporous channels of zeolites framework, together with Brønsted and Lewis acid sites, promotes polymerisation and aromatisation reactions, generating carbonaceous deposits. These deposits accumulate and mask pores, reducing the specific surface area by covering active sites, ultimately decreasing catalytic performance and product yield [15]. To reduce the coke formation, literature shows that co-current feeding of O_2 is required since it allows continuous consumption of the carbonaceous species [16,17].

Following acrolein formation, MoVO efficiently catalyses its oxidation to acrylic acid and is widely used in industrial propylene-to-acrylic-acid processes [18,19]. Chen et al. [20,21] reported that different Mo_3VO_x phases (orthorhombic, trigonal, tetragonal, and amorphous) achieved over 90% yield in the selective oxidation of acrolein to acrylic acid, with only microstructural differences affecting performance. Among the phases, orthorhombic Mo_3VO_x (Ortho-Mo_3VO_x) has gained much attention due to its outstanding catalytic performance in selective oxidation [22–24]. As for the case of oxidative coupling of methane to ethylene, it has been shown that the selectivity to ethylene is governed by either lattice oxygen available at the catalyst surface or molecular oxygen provided via air stream [25]. To enable this mechanism, oxygen content at the reaction site can be minimised by distributing oxygen feed through the reactor bed by means of multiple inlet points, or a porous membrane that could serve as an oxygen distributor as in the case of selective propane-to-acrolein oxidation [26]. Studies show that a distributor inside the reactor provides uniform oxygen within the reaction zone, thereby enhancing thermal management and selectivity towards desirable products [27,28]. The oxygen supplied through the membrane promotes partial oxidation, while the balance between lattice oxygen mobility and reoxidation rate governs selectivity and suppresses overoxidation to CO/CO_2 (CO_x) [29–31]. Prior studies indicate that MoVO maintains stable catalytic activity and undergoes slow deactivation by oxygen mobility and water effect [32,33]. Mechanistically, water enhances the reaction by adsorbing on the oxide surface to form hydroxyls, which activate acrolein via hydration or proton transfer, accelerating the rate-limiting step while maintaining high selectivity [34]. Water improves conversion and selectivity by suppressing coke formation, promoting catalyst reoxidation and mitigating total oxidation [35].

In a previous work from the authors [9], the main study focused on catalyst screening, configuration and formulation, catalyst characterisation, operating window identification, and understanding the effect on acrylic acid selectivity and yield related to enhancing catalyst design. In addition, the reaction mechanism to understand the role of the catalytic components, risk for degradation and material regeneration, was explored. In the present study, the combined use of HZSM-5(200) and orthorhombic MoVO (Ortho-MoVO) catalysts is investigated for the first time in a novel membrane-assisted reactor (MR) configuration. This new configuration, which has never been investigated in literature, intensifies the process by using a porous membrane integrated within the reactor for the oxidation of acrolein (intermediate) via selective oxygen distribution (via air). Moreover, both catalysts developed and optimised in the previous work [9] are scaled up to large batches (×10 times) compared with the performance at a small scale (as packed-bed reactor) and in the presence of the membrane. In order to optimise the operating conditions, the effect of temperature, gas hourly space velocity (GHSV), molar oxygen-to-glycerol (O_2/G) ratio, and feed-to-membrane (F/M) ratio are examined. A systematic design of experiments using statistical modelling response surface methodology (RSM) established reliable correlations between the operating variables (such as temperature, pressure) and the measured responses (conversion, selectivity) [36].

Additionally, an optimisation study was carried out to define an operational region that enhances acrylic acid formation while maintaining high glycerol conversion and minimising complete oxidation to CO_x, thereby improving catalytic efficiency and process sustainability. Furthermore, catalyst stability and coke deposition studies were performed to understand its nature and composition after reaction.

2. Methodology

2.1. Materials and reagents

Glycerol (>99.5%) and HZSM-5(200) zeolite (SAR 200–400) were purchased from Thermo Fisher Scientific. Ammonium molybdate tetrahydrate was obtained from Fisher Scientific, while vanadyl sulfate hydrate (97.0%) and oxalic acid were sourced from Sigma-Aldrich. Silicon carbide pellets (F-24 mesh, coarse) were acquired from Clear Minerals.

2.2. Catalyst synthesis

The zeolite was calcined at 550 °C for 6 h, prior to the reaction. The dry zeolite was pelletised using a manual pelletiser with a mesh of 300–400 μm particle size. The oxidation catalyst (Ortho-MoVO) was synthesised via a hydrothermal method, following a similar process mentioned in previous work by Bansod et al. with a detailed description provided in SI [9,20].

2.3. Characterisation methods

The powder X-ray diffraction (XRD) patterns of all catalysts were recorded on a Panalytical X'Pert Pro diffractometer, featuring a copper line-focus X-ray tube and a nickel kβ filter (λ = 1.542 Å). Data acquisition was performed with a step size of 0.03° and angular scanning range (2θ) from 5° to 60°. The Fourier Transform Infrared (FTIR) spectra were recorded using a Bruker Vertex 70 FTIR spectrometer, with 256 scans collected at a resolution of 4 cm^{-1}. Scanning electron microscopy (SEM) was carried out on an FEI Quanta 250 system. Prior to SEM imaging, the samples were sputter-coated with a 10 nm Au/Pd layer to minimise charging effects. Transmission electron microscopy (TEM) was conducted using a TALOS microscope (Thermo Fisher Scientific) equipped with advanced imaging and analytical features. High-resolution TEM (HRTEM) was used to examine the crystalline structure and lattice arrangement, while high-angle annular dark-field (HAADF) imaging provided compositional contrast. Elemental composition and spatial distribution were analysed using scanning TEM coupled with energy-dispersive X-ray spectroscopy (STEM-EDS). Thermogravimetric analysis (TGA) of fresh and spent catalysts was conducted using a Shimadzu TGA-50 analyser to study the thermal stability. Approximately 20 mg of each sample was heated from ambient to 800 °C (HZSM-5(200)) and 600 °C (Ortho-MoVO) under a N_2 flow of 40 mL•min^{-1}. The temperature was ramped at 10 °C•min^{-1} to 300 °C and held for 1 h under N_2, then increased to 600 °C and maintained for another hour. In the case of

coke deposition study, air was used when the catalyst reached the maximum temperature (kept at constant temperature for 1 h to oxidise coke). Finally, the atmosphere was reverted back to N_2, and the temperature was raised to 800 °C and held for 1 h isothermally under both N_2 and air [37]. The amount of coke in the residue was obtained as the difference between the weight loss in N_2 and that of air as mentioned in Eq. (2).

$$\text{Amount of coke (\%)} = \frac{(y_1 - y_2)}{y_1} \times 100 \quad (2)$$

where y_1 and y_2 are initial and final weight in (mg) before and after the decomposition under N_2 and air, respectively.

The carbon-hydrogen-nitrogen (CHN) elemental analysis was carried out using a Thermo Flash Smart Elemental Analyser based on dynamic flash combustion. Accurately weighed samples in tin capsules were combusted in a quartz reactor at 900 °C under helium, with oxygen introduced to achieve rapid oxidation at 1800 °C. The combustion products (CO_2, H_2O, N_2) were passed over catalysts to ensure complete conversion and reduction, then separated chromatographically and detected by a thermal conductivity detector. Metal analysis (Mo and V) was performed using an inductively coupled plasma - optical emission spectroscopy (ICP-OES spectrometer Thermo iCAP 6300 Duo). Samples and reference standards were accurately weighed into glass digestion tubes, and four calibration standards (5–20 ppm) were prepared. Following acid digestion under appropriate conditions, all solutions were diluted with deionised water and transferred to volumetric flasks.

2.4. Catalytic testing, experimental set-up and analysis

The reaction was conducted in a tubular stainless-steel reactor (ID: 3 cm; L: 80 cm) experimental rig, as shown in Fig. 1. For the dehydration stage, 10 g of zeolite was mixed with 40 g of silicon carbide (SiC) pellets as an inert diluent, forming a packed-bed approximately 6 cm in length. Above this layer, 20 g of Ortho-MoVO catalyst was blended with 80 g of SiC and packed to a height of 18 cm for the subsequent oxidation step. The membrane reactor was manufactured by Eindhoven University of Technology in the NL (Inorganic Membrane Group of Prof. Gallucci).

The porous alumina membrane (L-18 cm, OD-1.3 cm; pore size 100 nm manufactured by Inopor® and provided by TU Eindhoven) was positioned on the top side of the reactor, as illustrated in SI Fig. S8. Air and N_2 were supplied through mass flow controllers (Bronkhorst, The Netherlands) along with glycerol or through the membrane (dashed line Fig. 1). The aqueous glycerol feed (10 wt%) was stored in a pressurised vessel and delivered to the reactor via a liquid flow controller, ensuring accurate dosing of the feed solution from the bottom of the reactor. The solution was preheated to 200 °C and mixed with N_2 using a control evaporator and mixer (CEM) before entering the reactor. In this study, single membrane testing and permeation measurements were not considered. This is because the membrane used for this study acts as a material (air/O_2) distributor. To validate the new membrane reactor concept, a study at the reactor level was required; therefore, an existing long ceramic-based membrane was used instead of a new one, specifically developed for this application.

Heating tapes were installed along the feed and outlet lines to prevent condensation of glycerol vapour. Pressure gauges and transducers were positioned along the process line to monitor pressure drops during operation. Reactor temperature was measured at three axial positions along the bed.

The product stream recovered from top of reactor and passed through two consecutive cold traps maintained at 0 °C, and liquid samples were collected hourly. The condensed products were analysed using a Dionex Ultimate 3000 HPLC system equipped with an Aminex organic acid column (ID = 1 cm, L = 15 cm) with both UV and refractive index (RI) detectors (detailed information with product calibration in SI Fig. S3 and Table S3). The mobile phase consisted of 5 mM H_2SO_4, operated at a constant flow rate of 0.3 mL min^{-1} with an injection volume of 10 µL. Gas-phase products were monitored online using a mass spectrometer (MS) connected directly to the reactor outlet.

The catalyst was activated at 300 °C under atmospheric pressure for 1 h with N_2 and then maintained desired temperature of (260–300 °C) for 1 h to stabilise it. The reaction was carried out for 7 h time-on-stream (TOS). Glycerol conversion, product yield and selectivity, respectively, were calculated using Eqs. (3), (4) and (5) as mentioned below.

$$\text{Glycerol conversion (\%)} = \frac{\text{moles of glycerol}(C_3H_8O_3)\text{ reacted}}{\text{moles of glycerol}(C_3H_8O_3)\text{ fed}} \times 100 \quad (3)$$

$$\text{Yield (\%)} = \frac{\text{moles of product formed } (P_i)}{\text{moles of glycerol}(C_3H_8O_3)\text{ fed}} \times 100 \quad (4)$$

$$\text{Selectivity (\%)} = \frac{\text{moles of product formed } (P_i)}{\text{moles of glycerol}(C_3H_8O_3)\text{ reacted}} \times \frac{x_i}{3} \times 100 \quad (5)$$

where x_i, represents the number of carbon atoms of the respective product (P_i) to discriminate the product distribution against the carbon conversion of the original feedstock.

The carbon balance was calculated as the sum of residual glycerol (C_{Gly}) and total detected products in the liquid (C_{liquid}) and gas (C_{gas})

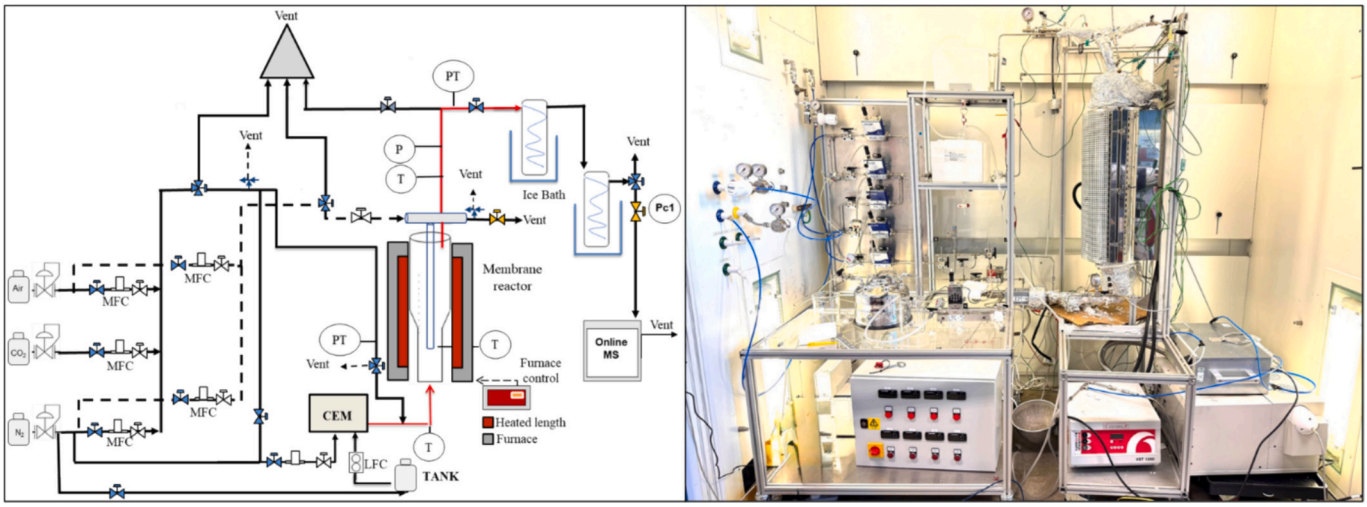

Fig. 1. Schematic of experimental setup (left) and the rig (right).

phases (Eq. (6)) with more details provided in SI Eq. (1). The difference between inlet and outlet was used to estimate the amount of coke deposited/consumed.

$$\text{Carbon balance} = C_{Gly} + C_{liquid} + C_{gas} \quad (6)$$

Two reactor configurations have been compared (Fig. 2): i) in the first case, a conventional packed-bed reactor with oxygen (in air) fed along with diluted glycerol from the reactor inlet as shown in Fig. 2(a), PBR; ii) in the second case, a membrane is also inserted in the top section of the catalytic bed (Ortho-MoVO + SiC) and air is fed through the membrane and from the reactor inlet together with glycerol as shown in Fig. 2(b), MR.

The key parameters used to investigate the effect on the glycerol to acrylic acid process are considered in Table 1. For the MR configuration, the air feed from the membrane (M) and the reactor inlet has been varied in the ratio of 90:10, 50:50, 10:90.

Table 1
List of parameters: temperature, GHSV and O_2/G ratio.

Temperature (°C)	GHSV (h^{-1})	O_2/G ratio (–)
260	553	9.5
280	1935	14
300	3318	18.5

Each parameter was changed independently while maintaining the constant standard operating conditions for the others, so that the effect on acrylic acid selectivity and conversion can be recorded.

2.5. Design of experiment and optimisation

The Design of Experiment (DoE) and related optimisation employed

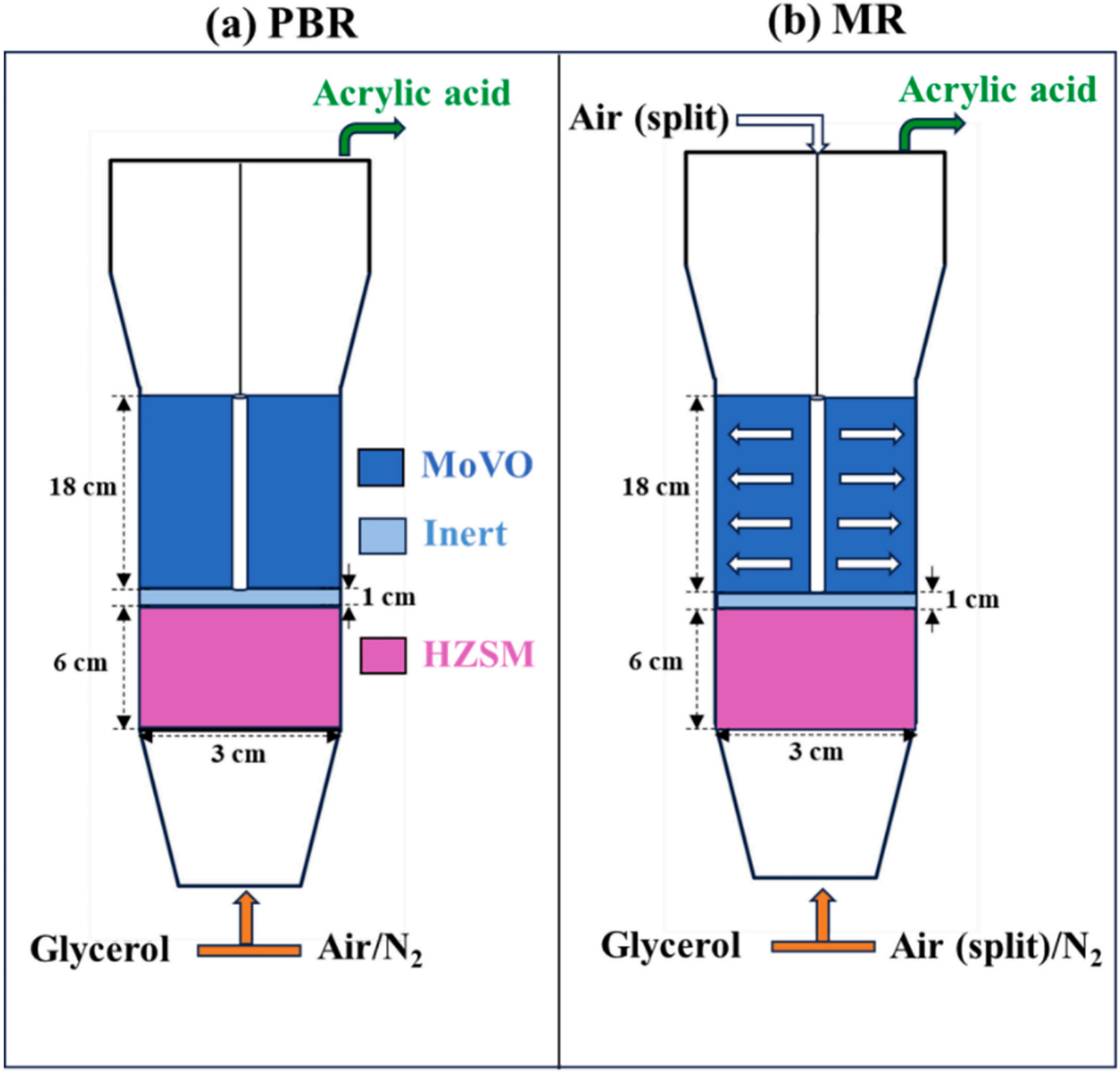

Fig. 2. Schematic of (a) conventional packed-bed reactor (PBR) and (b) membrane reactor (MR).

in this study is carried out using Minitab software version 22.2, using a response surface methodology (RSM) approach that generates a polynomial or linear model aids in experimental design to correlate independent variables with the response parameters and identify optimum operating conditions. For the PBR configuration, 15 experiments were conducted (Table S1 in the SI), while 27 experiments were performed for the MR configuration (Table S2 in the SI). The experimental data were subsequently used to develop a model aimed at maximising glycerol conversion and acrylic acid selectivity while minimising CO_x selectivity under favourable conditions. The DoE was employed to quantitatively compare reactor configurations at increased scale and to identify the coupled effects of GHSV, O_2/G and the newly introduced F/M ratio on performance under distributed oxygen feeding. The complete dataset is provided in the SI along with regression analysis, ANOVA, uncoded regression equations and optimised solution.

3. Results and discussion

3.1. Effect of reaction parameters

3.1.1. Feed-to-membrane (F/M) ratio

The membrane reactor configuration enables flexible oxygen distribution by feeding air through both the reactor inlet and the membrane. To optimise this distribution, the feed-to-membrane (F/M) ratio was systematically varied while maintaining constant total air flow. Fig. 3b presents the effect of F/M ratio on glycerol conversion and product selectivity (detailed data in Table S7 in the SI). At a fixed GHSV of 1935 h^{-1}, O_2/G ratio of 14:1, and reaction temperature of 280 °C, varying the F/M ratio altered the balance between oxygen transport and reactant residence time. When 10% of the air was directed to the membrane side (F/M = 90:10), the acrylic acid selectivity slightly rises (50.4%) as compared to PBR (48.6% as presented in Fig. 3a), accompanied by a notable rise in CO_x selectivity (22.6%). At balanced F/M = 50:50, the acrylic acid selectivity reached its maximum value of 58.7%, with CO_x selectivity decreasing to 13.9% compared to the use of a 90:10 ratio. This configuration provided an optimal oxygen flux across the distributor wall, ensuring sufficient oxidation for acrolein conversion while suppressing overoxidation. Conversely, at increased membrane flow (F/M ratio = 10:90) the results reduced acrylic acid selectivity to 56.2% and slightly increased CO_x to 14.3% compared to 50:50, suggesting that excessive air to the catalyst side disturbed the controlled oxygen diffusion mechanism [26,27]. A similar increase on CO_x selectivity was recorded also in previous work in case of low O_2/G ratio (9.5:1 and 14.2:1 vs 4.7:1) [9].

This testing campaign suggests that there is an optimum acrylic acid production with respect to the oxygen supply.

The selective oxidation of acrolein to acrylic acid is first order with respect to acrolein concentration [34]. Increasing the O_2 partial pressure (via air) in excess promotes parallel and consecutive deep-oxidation pathways; this highlights the importance of maintaining moderate local oxygen partial pressures to preserve acrylic acid selectivity [38]. The main positive aspect of this design is that the oxygen (from air) permeates along the axial length of the reactor while keeping a low oxygen partial pressure, which favours acrolein to acrylic acid formation over its combustion or formation to CO_x or other by-products in a kinetic-controlled mechanism of selective oxidation [39]. This is possible because in the case of MR, oxygen is distributed uniformly along the reactor length, preventing local O_2 spikes and maintaining consistent O_2 availability to match the kinetic order, thereby enhancing acrylic acid selectivity [40,41].

Given that the best performance was obtained by splitting air between reactor feed and membrane (F/M = 50:50), the comparison with the packed-bed configuration (without membrane) in the next sections is carried out using this case as the reference for the membrane reactor.

3.1.2. Reaction temperature

The catalytic performance on GTA process was examined at three distinct temperatures (260, 280, 300 °C) for both the PBR and MR configurations, as shown in Fig. 4 (also shown in Table S4 in SI). All conditions show consistently high (>94%) glycerol conversion, indicating temperature primarily influences product selectivity rather than overall conversion. In PBR, Fig. 4a, raising the temperature from 260 °C to 280 °C increases selectivity to acrylic acid from 42.5% to 48.6%. However, further increasing the temperature to 300 °C causes a drop in acrylic acid selectivity to 31.0%. This indicates an optimal temperature around 280 °C for acrylic acid formation in the PBR, beyond which selectivity declines. Roug Liu et al. also reported similar behaviour for GTA process [30], which is explained by a significant rise in C1 by-products via C—C bond breakage [42], confirmed by CO_x selectivity (48.3% and 39.5%) for both the case PBR and MR, respectively. The best performance was found at 280 °C, attaining 48.6% in the PBR and a notably higher 58.7% in the MR-assisted system.

The distribution of by-products explains the reaction pathway, as reported previously by Bansod et al. [9]. Acetic acid, the main secondary

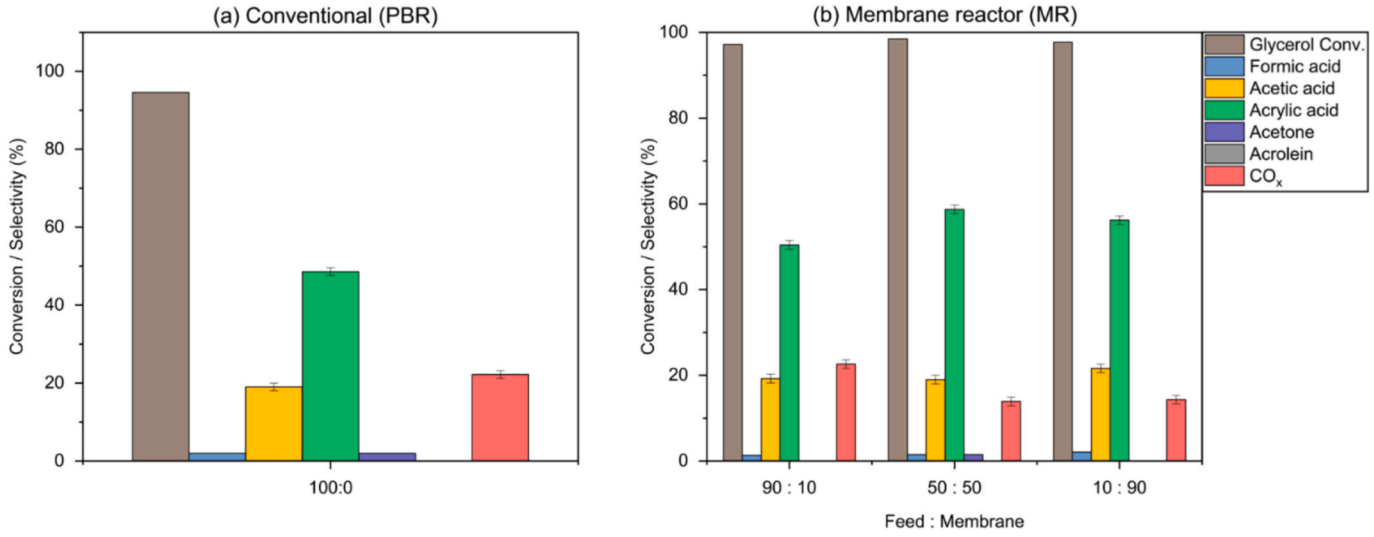

Fig. 3. Effect of feed-to-membrane ratio on conversion and selectivity of GTA process for a) PBR and b) MR. Reaction conditions: dehydration catalyst HZSM-5(200), and oxidation catalyst Ortho-MoVO; temperature 280 °C; GHSV 1935 h^{-1} and feed composition (mol%) glycerol/O_2/H_2O/N_2 = 1/14/45.2/80.9. Conversion and selectivity data were taken after 3 h TOS.

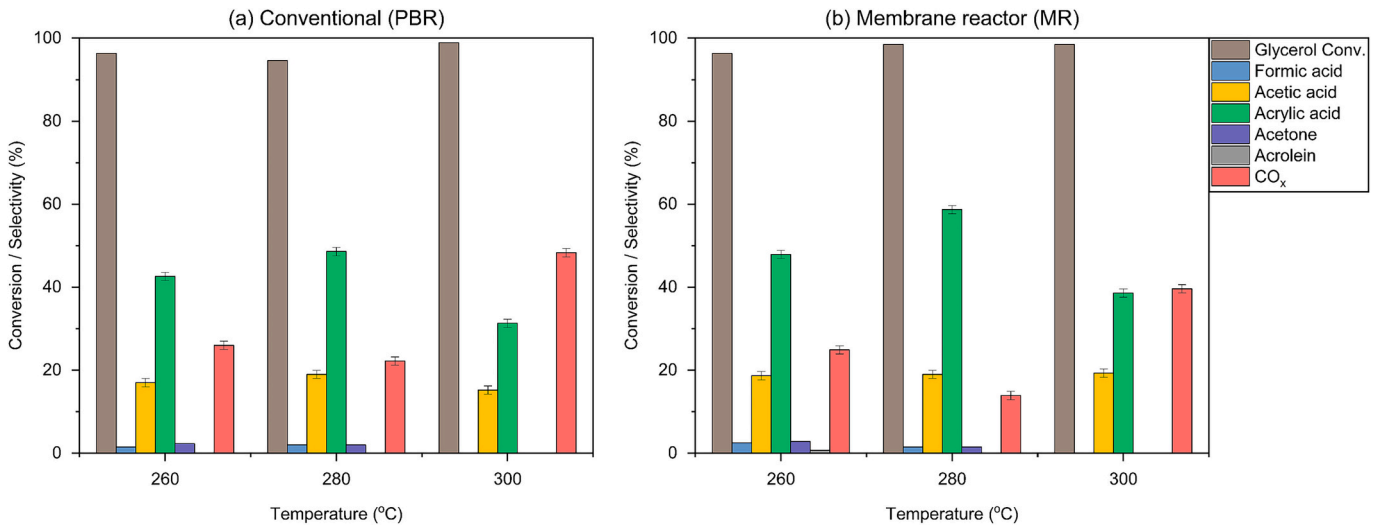

Fig. 4. Effect of temperature on conversion and selectivity of GTA process for a) PBR and b) MR. Reaction conditions: dehydration catalyst HZSM-5(200), and oxidation catalyst Ortho-MoVO; GHSV 1935 h^{-1}; feed-to-membrane ratio = 50:50 (MR) and feed composition (mol%) glycerol/O_2/H_2O/N_2 = 1/14/45.2/80.9. Conversion and selectivity data were taken after 3 h TOS.

product after acrylic acid, showed stable selectivity of 15–21.6% in both reactor configurations, without decomposition to lighter gases. Formic acid displayed strong temperature dependence, being prominent at lower temperatures but sharply decreasing at 300 °C [43,44].

Fig. 5 compares the temperature profiles during the GTA process. For PBR a sudden rise of approximately 10 °C is observed at the beginning of the reaction (Fig. 5a), followed by stabilisation at an average temperature of 287 °C with reference to the Ortho-MoVO layer (T3) located at the midpoint of the membrane. This behaviour indicates the exothermic nature of the oxidation of acrolein to acrylic acid. While, in the case of the MR (Fig. 5b), the temperature is maintained around 283.5 °C, with a smaller rise of about 7–8 °C at the beginning of the reaction, demonstrating improved thermal management through distributed air feeding. This reactor design could also help to reduce hot-spot formation, enhance reaction stability, and consequently improve product selectivity in MR [45].

3.1.3. Gas hourly space velocity (GHSV)

Fig. 6 shows three variations of GHSV (553, 1935, 3318 h^{-1}) that influenced glycerol conversion and acrylic acid selectivity. At the lowest GHSV (553 h^{-1}), the extended residence time ensured complete glycerol conversion in both PBR (Fig. 6a) and MR (Fig. 6b). Increasing GHSV led to a gradual decline in conversion, reflecting the inverse relationship between residence time and contact efficiency. The prolonged contact time at low GHSV increased the CO_x selectivity at the expense of the acrylic acid selectivity, which is limited to 38.0% and 39.5% for the PBR and MR, respectively.

At an intermediate GHSV of 1935 h^{-1}, the residence time remained sufficient for near-complete glycerol conversion (94.6% PBR, 98.5% MR) and prevented acrolein decomposition that effectively limits overoxidation. Consequently, acrylic acid selectivity improved significantly, reaching 58.7% in the MR, accompanied by a marked suppression of CO_x formation (13.9%).

At the highest GHSV (3318 h^{-1}), glycerol conversion declines slightly (93.6% PBR, 92.5% MR) due to reduced contact time between reactant and catalyst surface required for complete transformation of intermediates, as well as possible channelling arising from changes in flow pattern [46]. Under this condition, acrylic acid selectivity also decreased to (38.5% in the PBR, 48.6% in the MR), while CO_x formation increased correspondingly, indicating enhanced side reactions. Similar

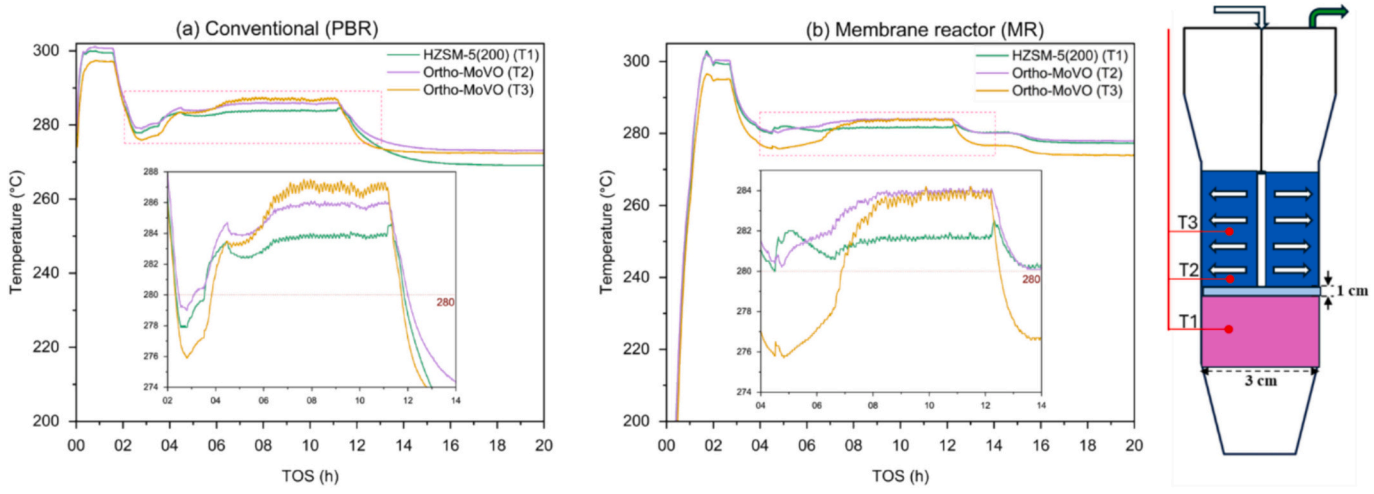

Fig. 5. Temperature profiles (a) PBR and (b) MR over TOS for a temperature of 280 °C GHSV 1935 h^{-1}; feed-to-membrane ratio = 50:50 (MR) and feed composition (mol%) glycerol/O_2/H_2O/N_2 = 1/14/45.2/80.9; three thermocouple positions are shown: T1, T2, and T3, distributed axially across the catalyst bed (illustrated in the schematic on the right).

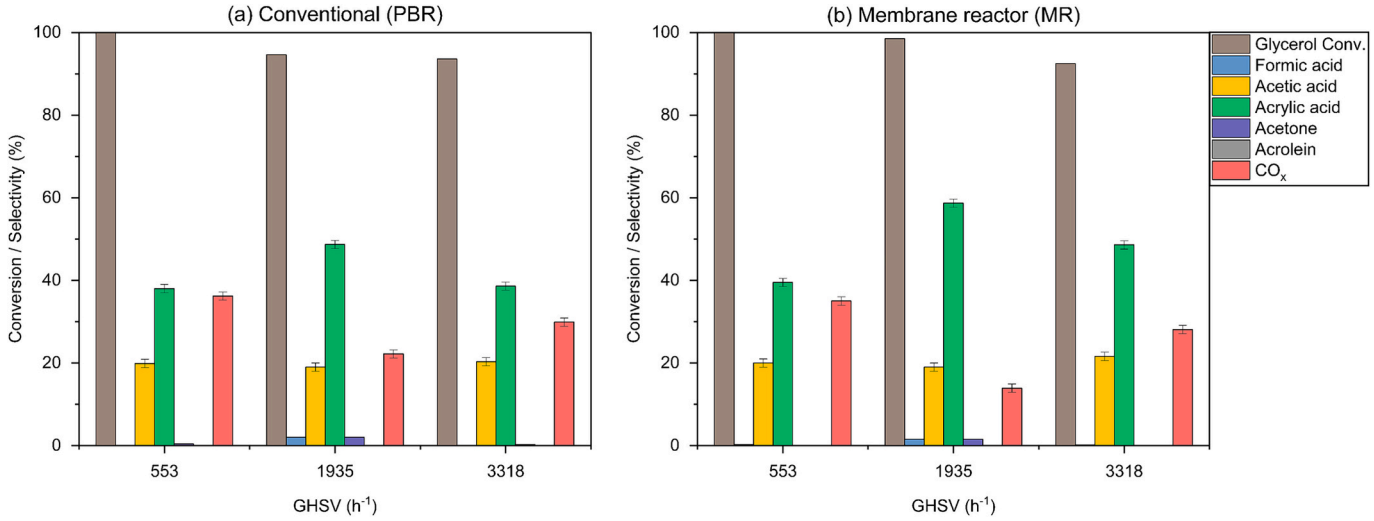

Fig. 6. Effect of GHSV on conversion and selectivity of GTA process for a) PBR and b) MR. Reaction conditions: dehydration catalyst HZSM-5(200), and oxidation catalyst Ortho-MoVO; temperature 280 °C; feed-to-membrane ratio = 50:50 (MR) and feed composition (mol%) glycerol/O_2/H_2O/N_2 = 1/14/45.2/80.9. Conversion and selectivity data were taken after 3 h TOS.

observations were made in Juliana et al. [42], indicating the impact of optimal GHSV in terms of acrylic acid yield [47].

3.1.4. Oxygen-to-glycerol (O_2/G) ratio

Fig. 7 (also shown in Table S6 in SI) illustrates the variation of three different values of O_2/G (9.5:1, 14:1, and 18.5:1) ratio, in which conversion is almost constant in both cases. However, in PBR (Fig. 7a), the lowest O_2/G ratio of 9.5:1 showed the highest acrylic acid selectivity of 50.9%. This decrease was accompanied by a rise in CO_x formation (from 20.1% to 27.3%), indicating that excess oxygen promotes overoxidation of intermediate species, thereby leading to less selective distribution of products [42]. Glycerol-rich feed can accelerate catalyst deactivation by promoting coke deposition and accumulation on the catalyst surface [44]. However, higher oxygen concentration is required to maintain active surface sites and improve its stability despite the negative effect on CO_x selectivity [30].

The MR (Fig. 7b) exhibited a contrasting trend, acrylic acid selectivity not only exceeded that of the PBR system across all oxygen ratios but also peaked at an intermediate ratio of 14:1 (58.7%) with a comparatively low CO_x selectivity (13.9%). At the lowest ratio (9.5:1), selectivity remained high (57.0%), while further increasing air with O_2/G ratio 18.5:1 decreased acrylic acid selectivity to 53.6% and increased CO_x to 19.4%. These results suggest that above 14:1 the amount of oxygen made available during acrolein oxidation is not limiting the partial/total combustion reaction as experienced for other cases at a lower oxygen-to-glycerol ratio. Moreover, in the MR, the same selectivity of the two cases at oxygen-to-glycerol ratio 9.5:1 and 14:1 is beneficial since it would allow operating the process with more air, further suppressing coke formation in the first part of the bed (glycerol dehydration).

3.1.5. Optimum conditions

To determine the optimal operating parameters for the GTA process, an RSM based on Box Behnken method was employed. Detailed results are provided in the SI (Figs. S9 and S11). The regression models developed for the PBR system demonstrated excellent statistical significance and predictive capability, with R^2 values above 99.2% and adjusted R^2 exceeding 97.7% for all three responses. Analysis of variance (ANOVA) confirmed that temperature and GHSV were the most influential factors ($p < 0.01$), while O_2/G comparatively had a minor

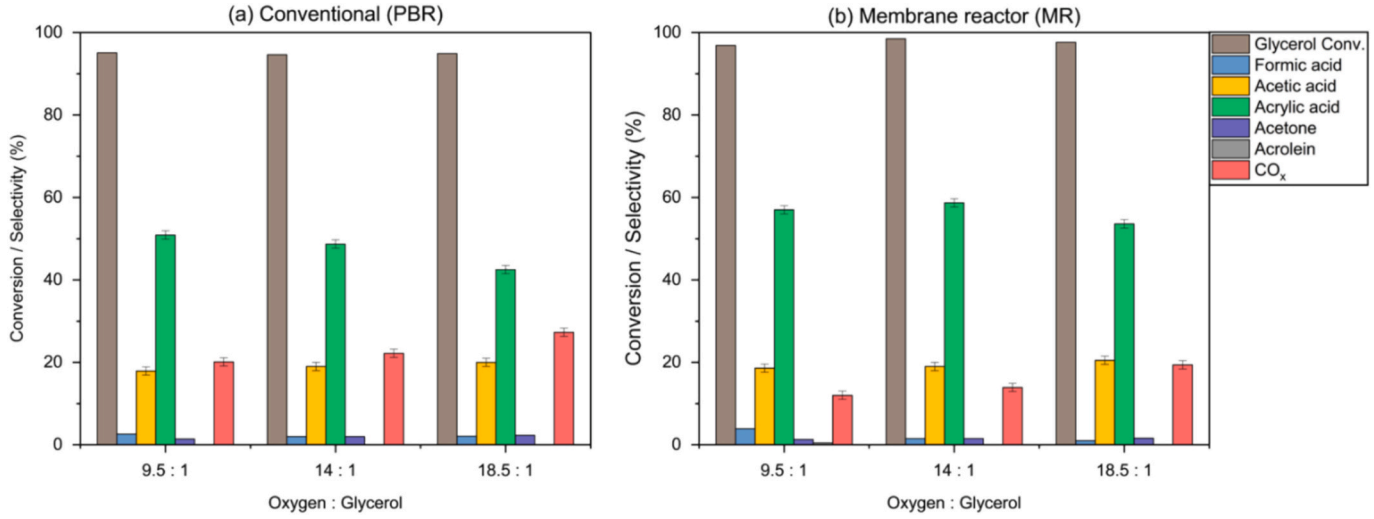

Fig. 7. Effect of O_2/G on conversion and selectivity of GTA process for a) PBR and b) MR. Reaction conditions: dehydration catalyst HZSM-5(200), and oxidation catalyst Ortho-MoVO; temperature 280 °C; GHSV 1935 h^{-1} and feed-to-membrane ratio = 50:50 (MR). Conversion and selectivity data were taken after 3 h TOS.

effect. The predicted optimum conditions were 276.97 °C, GHSV = 1893.9 h^{-1}, and $O_2/G = 9.5$, resulting in a glycerol conversion of 95.9%, acrylic acid selectivity of 49.2%, and CO_x selectivity of 22.2% with a desirability of 0.75 (more details please refer SI Fig. S10).

For the MR configuration, inclusion of the F/M ratio as an additional variable with model accuracy (R^2 = 98.1–96.75%, adjusted R^2 > 92.95%). ANOVA revealed that temperature, GHSV, and O_2/G were statistically significant ($p < 0.05$). The quadratic effects of temperature and GHSV were dominant for both acrylic acid and CO_x selectivity, indicating non-linear behaviour. The numerically optimised conditions are: temperature = 280 °C, GHSV = 1838 h^{-1}, $O_2/G = 13.68$, and F/M = 50.4%. Under these conditions, the model predicts glycerol conversion of 98.9%, acrylic acid selectivity of 58.7%, and CO_x selectivity of 13.9% with an overall desirability value of 0.75, as summarised in Table 2 (more details are provided in the SI, Fig. S12 and corresponding contour plots are shown in Fig. S13). Hence, the acrylic acid selectivity improves by 20.16% using a membrane reactor. Notably, the use of a membrane reactor for propylene-to-acrolein production (via oxidation) has obtained similar results as reported by O'Neill and E.E. Wolf [48], suggesting that this concept can also be applied to the traditional (fossil-fuel) route to acrylic acid by using a dual-bed membrane reactor and providing oxygen throughout the reactor length.

Compared to the previous work [9], the optimised configuration presents the same optimum temperature (280 °C), but it differs on selectivity/conversion trends due to the effect on the scale of the reactor dictated by the GSHV and the air feeding mechanism (membrane vs inlet reactor) while an optimum O_2/G ratio (14:1) is obtained compared to a constant trend noted in [9].

3.1.6. Long-term stability test

The continuous testing of the catalyst system (HZSM-5 (200) + Ortho-MoVO) was carried out for 44 h over a period of 7 days under the optimised reaction conditions shown in Fig. 8. Prior to each run, the reactor was preheated to 300 °C for 3 h. During the stability test, liquid samples were collected every hour, and the furnace temperature was maintained at 280 °C overnight to ensure consistent reaction conditions, including GHSV, O_2/G ratio and membrane-to-feed (F/M) ratio. Acrylic acid selectivity increased from 46% to approximately 58% during the first three days of operation, reflecting catalyst activation and stabilisation. Between 12 and 21 h, selectivity remained steady, confirming that the catalyst was fully active during this period. After 22 h, a gradual decline in selectivity was observed. This marks the onset of coke accumulation, which progressively blocks acid sites on HZSM-5(200), reducing acrolein formation and consequently lowering acrylic acid selectivity. A significant loss in selectivity was recorded on day 5 (after 28 h of cumulative operation), attributed to increased coke deposition, pore blockage and reduced accessibility of active sites. These effects limit acrolein production and therefore suppress acrylic acid formation. The quantitative analysis of the stability data reveals a biphasic deactivation pattern: acrylic acid selectivity remained relatively stable at 58–60% for approximately the first 22 h of operation, followed by a sharp decline to ~25% by 44 h (1.5% per hour decrease). In contrast, glycerol conversion remained consistently above 95% throughout the entire test period. This behaviour indicates that deactivation selectively affects the formation or conversion of acrolein (the intermediate) rather than glycerol activation. The spent material was further analysed with SEM, XRD, FTIR, CHN and TGA analyses, as discussed in Section 3.2. Regeneration of the spent material at 350 °C did not result in any appreciable recovery of activity, consistent with the TGA results (Fig. 11) indicating that effective coke removal from zeolites requires temperatures of >600 °C.

Table 2
Optimised parameters and response factors predicted via DoE vs experimental values.

Parameters	Optimised (predicted via DoE)		Experimental	
	PBR	MR	PBR	MR
Temperature (°C)	276.9	280.0	276.9	280.0
GHSV (h^{-1})	1893.9	1838	1893.9	1838
O_2/G ratio	9.5	13.7	9.5	13.7
F/M ratio	–	50.4	–	50.4
Glycerol conversion (%)	95.9	98.9	94.1	97.0
Acrylic acid selectivity (%)	49.2	58.7	47.6	57.2
CO_x selectivity (%)	22.2	13.9	20.3	14.0

3.2. Characterisation of spent HZSM-5(200) and Ortho-MoVO

The XRD patterns of the spent zeolite after stability test (Fig. 9a) was compared with reference to the fresh sample (Fig. S17, SI) [9]. The spent material retains a similar characteristic MFI reflections with peaks observed in between 2θ 7–9°, and 23–25° [49]. However, the peak intensities decrease significantly, specifically at 7.99°, 8.86°, 24.0° 24.7°. This attenuation of maxima indicates a loss of crystallinity and partial framework degradation, reducing the availability of well-defined acid sites required for glycerol dehydration to acrolein and thereby lowering acrylic acid selectivity during long-term operation.

In the case of fresh Ortho-MoVO, as shown in Fig. 9b (SI Fig. S17b), the spent material exhibits an almost identical XRD pattern to the fresh sample and retained crystallinity of an orthorhombic structure after reaction. The positions, relative intensities and widths of the main reflections at 2θ = 6–7°, 22° and 45° match the orthorhombic reference pattern and remain unchanged after use. This confirms that the Ortho-MoVO structure is preserved during operation and crystallinity remains intact. Additionally, ICP-AES analysis of the fresh Ortho-MoVO catalyst noted 47.54 wt% Mo and 14.19 wt% V, confirms Mo/V molar ratio of 3.3, consistent with the findings of Chen et al. [20]. After the reaction, the spent material contained 45.83 wt% Mo and 11.03 wt% V with a small portion of material loss.

The SEM morphologies of the fresh and spent HZSM-5(200) and Ortho-MoVO catalysts are presented in Fig. 10. The fresh pelletised zeolites (Fig. 10a) exhibit a flat cylindrical-like structure with smooth homogeneous particle morphology (detailed TEM elemental mappings of fresh HZSM-5 (200) are shown in SI Fig. S14). However, the spent zeolites (Fig. 10b) retains the structure with partial fragmentation and surface roughing, with some cylindrical structure breaking into halves or quarters and layered structures appear damaged and irregular in shape. This also contributes to reduced catalytic performance during stability test. The fresh pelletised Ortho-MoVO catalyst, Fig. 10c, displays a thick, rod-like morphology and small broken fragments due to pelletisation [21] (more details in SI Fig. S15 with TEM micrographs showing elemental distribution of fresh Ortho-MoVO). The spent catalyst retains its structure, indicating morphology stability; however small agglomeration appears due to higher temperature (>300 °C). For more details, SI Fig. S16 shows increased sticky agglomeration with higher temperature.

Fig. 11 reports TGA analysis to quantify coke formation on the HZSM-5(200) and Ortho-MoVO catalysts after stability test. The fresh HZSM-5(200) exhibited an initial weight loss between 25 °C and 300 °C, as shown in Fig. 11a, associated with the removal of physisorbed moisture and weakly bound surface species. The subsequent isothermal hold at 300 °C for 1 h showed negligible change, confirming complete moisture removal. The spent HZSM-5(200) sample displayed an additional weight loss between 300 °C and 600 °C, followed by a 2 h isothermal period (1 h under N_2 and 1 h under air). At 600 °C, a weight loss of 2.37% under N_2 was attributed to the thermal decomposition or volatilisation of weakly bound organic species [15], while an additional 2.81% loss under air corresponded to coke combustion, indicating a total coke content of approximately 2.81% [37,50]. A subsequent temperature increase from 600 °C to 800 °C resulted in a minor weight loss of 0.3%, with negligible change observed during the isothermal holds under both N_2 and air. Also, at 800 °C, the material remained stable,

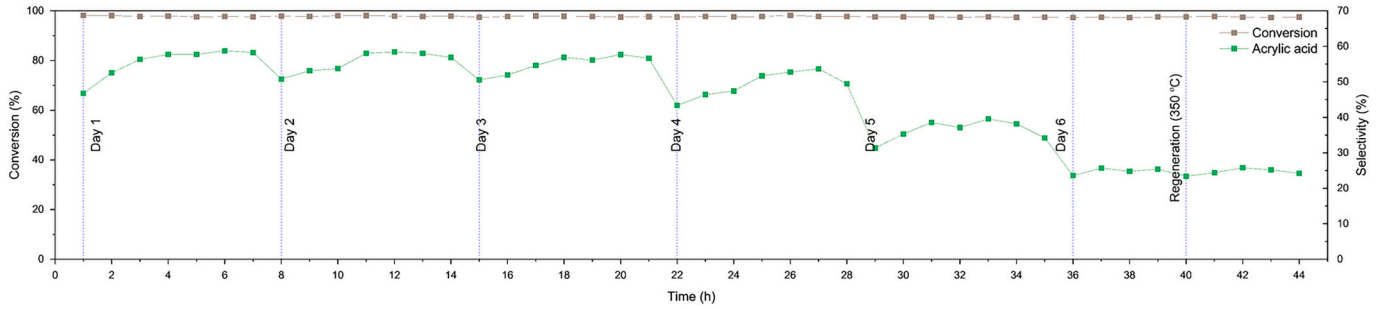

Fig. 8. Catalyst stability test during 44 h of continuous operation under optimised condition as 280 °C, GHSV 1935 h^{-1}, O_2/G ratio 14:1, and F/M ratio of 50:50.

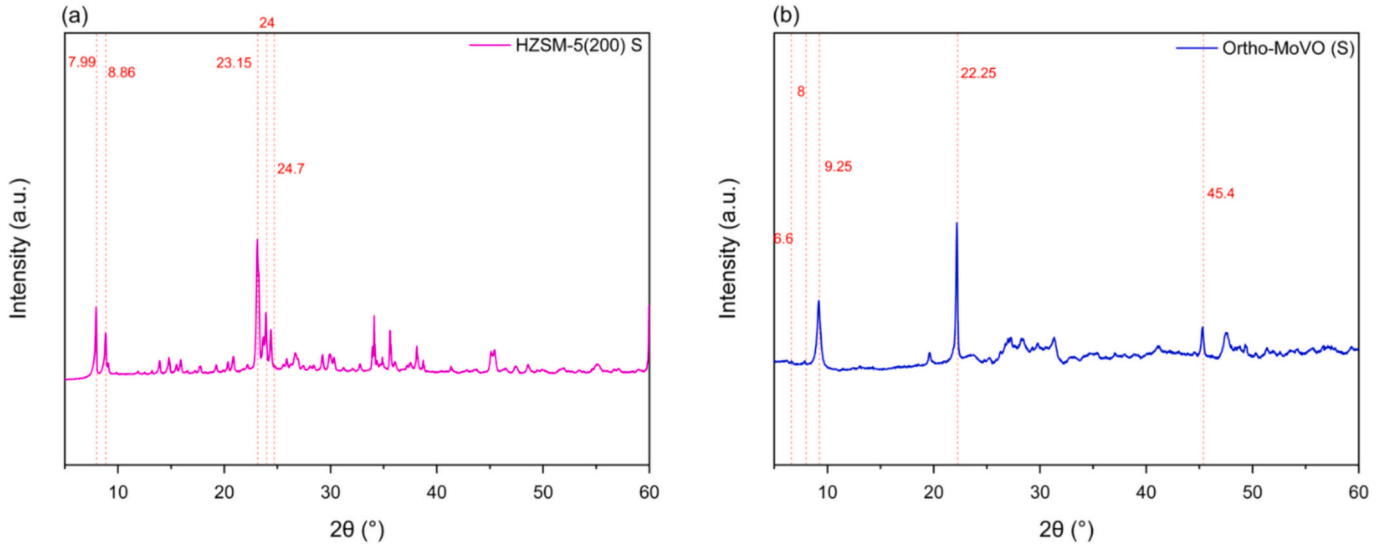

Fig. 9. XRD patterns of spent (a) HZSM-5(200) and (b) Ortho-MoVO.

showing no further decomposition at elevated temperatures, with more details in SI Table S8.

For Ortho-MoVO (Fig. 11b), the TGA profile between 25 °C and 300 °C shows a weight difference of 2.82% between the fresh and spent samples, signifying the loss of moisture and chemically exposed species. Upon heating from 300 °C to 600 °C and holding isothermally under N_2 for 1 h, a negligible weight change was observed, indicating the absence of coke formation, which is similar to observations reported in literature [44]. However, a slight increase in mass during the subsequent isothermal hold under air suggests possible reoxidation of V^+ and minor oxide loss from the Ortho-MoVO lattice during GTA reaction [51].

FTIR spectroscopy of fresh and spent zeolites after stability test was performed to investigate framework atomic group and vibration bands in Fig. 12a. The spectrum of the fresh sample is provided for comparison, while the spent exhibits characteristic absorption bands at 1070 cm^{-1}, which are noticeably weakened corresponding to external and internal asymmetric stretching, and features at 796 and 435 cm^{-1} attributed to external symmetric stretching [52,53]. The reduced band at 546 cm^{-1}, assigned to the double five-membered rings of MFI-type zeolites, reflects structural crystallinity [54]. Its reduced intensity in the spent sample indicates disruption in framework and reduced acid sites.

For Ortho-MoVO catalyst, Fig. 12b, the absorption at 870 cm^{-1} arises from Mo═O cis-dioxo stretching, while bands at 805, 710, and 646 cm^{-1} correspond to Mo–O–X (X = Mo, V) vibrations [55,56]. Additional features at 978 and 533 cm^{-1} are attributed to V═O and V–O–X (X═Mo) linkages [57]. Although band intensities decrease in the spent sample, the retention of key vibrations confirms that the Mo–O–V framework remains largely intact.

The CHN elemental analysis results for the fresh and spent HZSM-5 (200) and Ortho-MoVO catalysts are summarised in SI Table S9. The spent HZSM-5 (200) sample shows a notable increase in carbon content from 0.1 to 5.07 wt%, indicating significant coke deposition during the reaction and minute trace of hydrogen is observed. Converseley, the Ortho-MoVO catalyst exhibits a smaller increase in carbon (from 0.2 to 1.19 wt%) and little hydrogen, implying lower coke formation and better resistance to deactivation. Furthermore, N_2 was detected in Ortho-MoVO samples, from 0.1 wt% in the fresh catalyst due to N_2 purging in the preparation method to 1.95 wt% in the spent sample, likely because it was used as a carrier gas.

4. Conclusions and future work

This study investigated a continuous glycerol-to-acrylic acid chemical process via oxidative dehydration, using a membrane reactor (MR), and compared its performance against a conventional packed-bed reactor (PBR). The study demonstrated the feasibility of the concept, which resulted in improved performance in the final acrylic acid yield by using distributed oxygen feeding with a membrane. The presence of the membrane resulted in a maximum increase of a net +10% selectivity compared to the standard dual-bed PBR. The improved performances were confirmed also by varying key reaction parameters, including temperature, GHSV, oxygen-to-glycerol ratio, and feed-to-membrane ratio (specifically for MR), and examining their effect on the product distribution in both PBR and MR configurations. The highest acrylic acid selectivity of 58.7% was achieved under the optimised conditions (280 °C, GHSV 1935 h^{-1}, O_2/G ratio 14.1 and F/M ratio as 50:50). This work experimentally confirmed the hypotheses that in the presence of low oxygen concentration for the acrolein-to-acrylic acid reaction, the

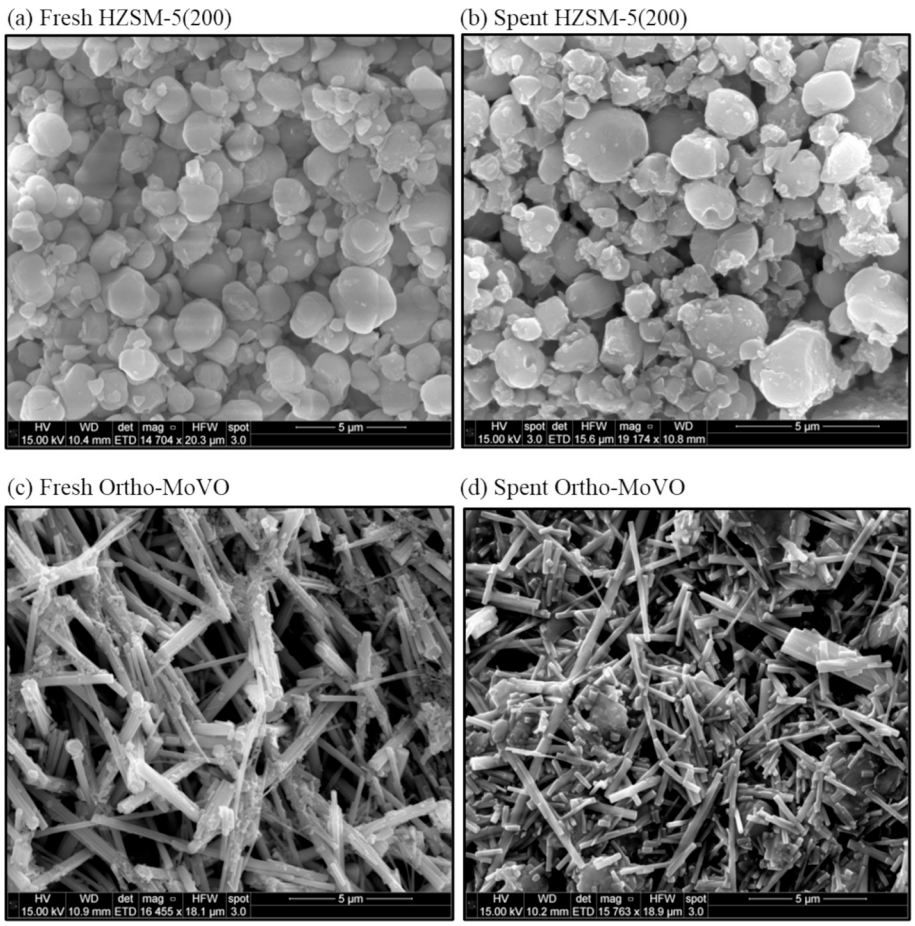

Fig. 10. SEM images of (a) fresh and (b) spent HZSM-5(200) catalyst and oxidation catalyst (c) fresh and (d) spent Ortho-MoVO.

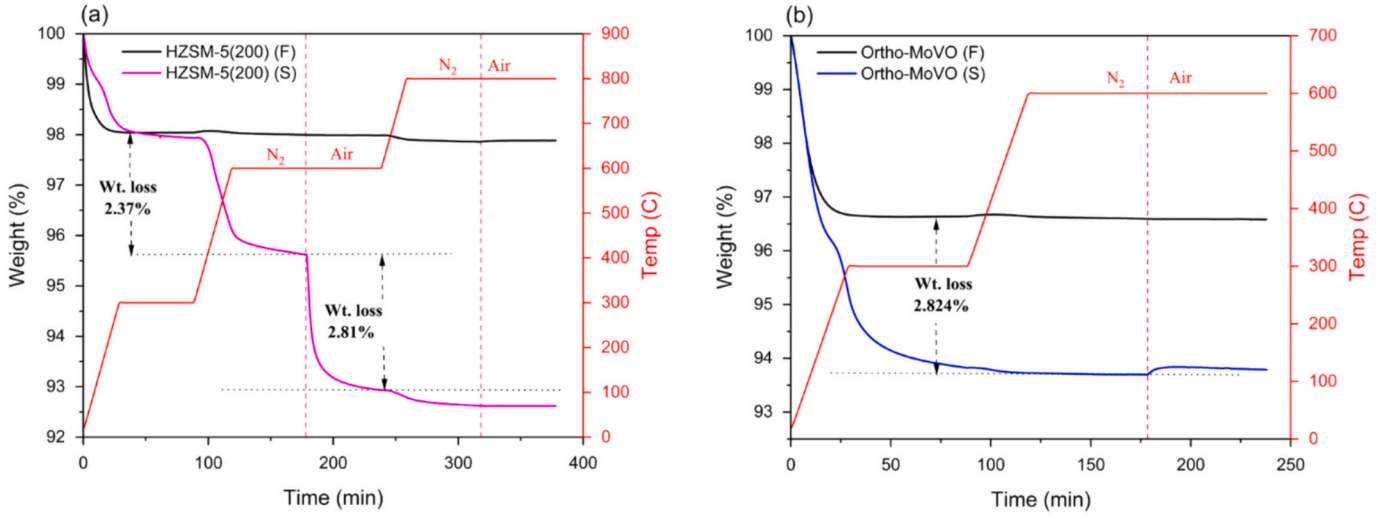

Fig. 11. TGA analysis of (a) HZSM-5(200) and (b) Ortho-MoVO for fresh and spent catalysts.

selectivity towards CO_x can be limited in favour of acrylic acid or other more valuable products. The improvement in acrylic acid selectivity translates to higher product yield per unit of glycerol feedstock, which could reduce downstream separation costs and improve overall process economics. At the reactor bed, the use of membrane also moderates the temperature rise, improving the heat management, preventing hot spots and controlling the selectivity towards acrylic acid (which decreases if the temperature is >280 °C). In addition, it is possible to use less oxygen, reducing the cost of production for both upstream and downstream of the reactor units. The development of specific membranes for this process could provide a foundation for selective oxidation strategies in sustainable engineering for acrylic acid manufacturing. Finally, the study focused on the stability test of the catalysts over 7 days of operation under reactive conditions, which highlighted the constant performance during the first 3 days while the catalyst (HZSM-5) was progressively deactivated after 28 h. Due to the thermal degradation of

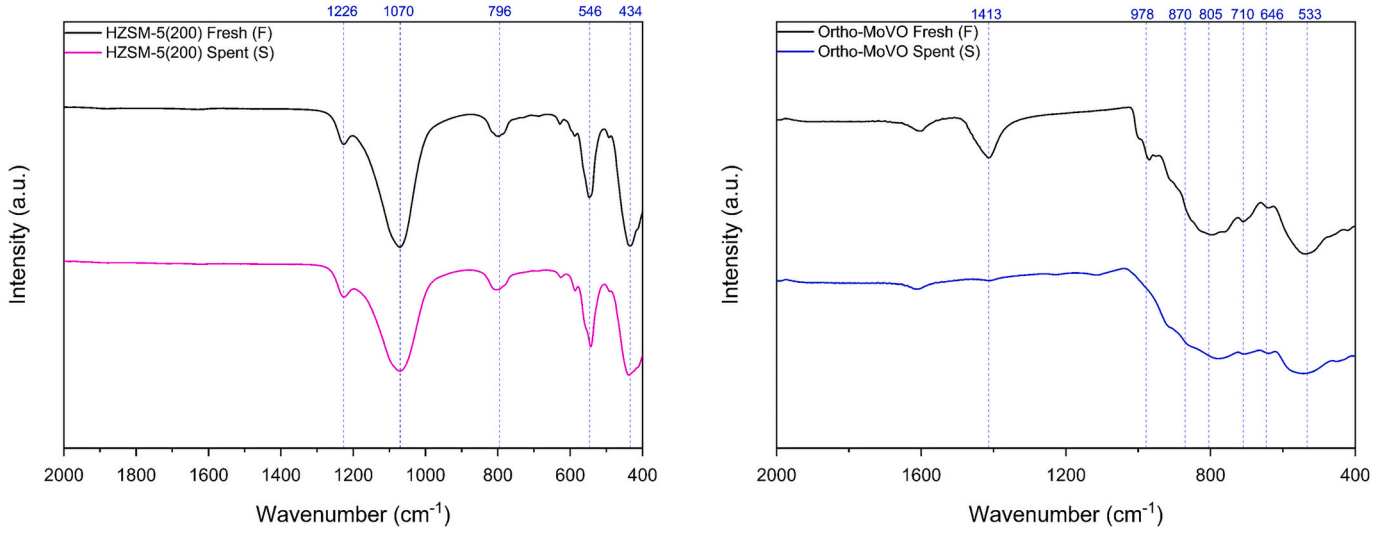

Fig. 12. FTIR spectra of fresh and spent (a) HZSM-5(200) and (b) Ortho-MoVO.

MoVO catalyst, regeneration with hot air could not be carried out >350 °C inside the reactor, hence the amount of coke removal was limited. This study demonstrated that further developments are required to find a suitable catalyst with higher resistance to carbon deposition. Zeolites are thermally robust but suffer from coke deposition; this can be minimised through regeneration. If the thermal stability of Ortho-MoVO or amorphous-MoVO phase can be enhanced to 600 °C, regeneration would be feasible in a single reactor, as most coke can be removed at this temperature. In terms of membrane reactor performance, the design and engineering of a new class of membranes to selectively separate oxygen from air could improve the viability of the process. Such a study would also require an in-depth analysis of the impact of operating pressure, which may play a relevant role in the kinetics and compactness of the equipment. Finally, the costs of the downstream purification under new and higher acrylic acid yield should be assessed and compared with standard processes.

Abbreviations and symbol

GTA	Glycerol To Acrylic acid
SAR	Silica to Alumina Ratio
HZSM-5 (200)	Zeolite Socony Mobil-5 protonated form (Silica to Alumina ratio 200)
MoVO	Molybdenum Vanadium Oxide
Ortho-MoVO	Orthorhombic-Molybdenum Vanadium Oxide
MR	Membrane Reactor
PBR	Packed Bed Reactor
GHSV	Gas Hourly Space Velocity
DoE	Design of Experiments
CO_x	Carbon Oxides (CO and CO2)
XRD	X-ray Diffraction
FTIR	Fourier Transform Infrared Spectroscopy
SEM	Scanning Electron Microscopy
TEM	Transmission Electron Microscopy
HRTEM	High Resolution Transmission Electron Microscopy
HAADF	High Angle Annular Dark Field
STEM-EDS	Scanning Transmission Electron Microscopy-Energy Dispersive x-ray Spectroscopy
SAED	Selected area electron diffraction
TGA	Thermogravimetric Analysis
CHN	Carbon Hydrogen Nitrogen
ICP-OES	Inductively Coupled Plasma - Optical Emission Spectroscopy
SiC	Silica Carbide
SI	Supporting Information
CEM	Control Evaporator Mixer
HPLC	High Pressure Liquid Chromatography
MS	Mass Spectrometer
TOS	Time On Stream
RSM	Response Surface Methodology
O_2/G	Oxygen-to-Glycerol ratio
F/M	Feed-to-Membrane ratio
y_1	Initial weight (mg)
y_2	Final weight (mg)
°C	Temperature
N_2	Nitrogen
ΔH^0	Standard enthalpy change
CO	Carbon monoxide
CO_2	Carbon dioxide
h	Hours
μm	Micrometre
mL	Millilitre
min	Minute
Mo	Molybdenum
V	Vanadium
λ	Wavelength (Å)
θ	Diffraction angle
ID	Inner Diameter
OD	Outer Diameter
L	Length
x_i	Number of carbon atoms
P_i	Product species i
Δ	Difference
F	Fresh
S	Spent

CRediT authorship contribution statement

Prashant Pawanipagar: Investigation, Formal analysis, Data curation, Conceptualization, Writing – original draft. **Yash Bansod:** Investigation, Data curation, Writing – review & editing. **Umar Abubakar:** Investigation, Data curation, Writing – review & editing. **Hassan Alhassawi:** Investigation, Writing – review & editing. **Min Hu:** Investigation, Data curation, Writing – review & editing. **Christopher De leeuwe:** Data curation, Writing – review & editing. **Kamran Ghasemzadeh:** Methodology, Investigation, Data curation, Conceptualization, Writing – review & editing. **Carmine D'Agostino:** Supervision, Resources, Project administration, Funding acquisition, Writing – review & editing. **Vincenzo Spallina:** Supervision, Resources, Project

administration, Investigation, Funding acquisition, Data curation, Conceptualization, Writing – original draft.

Declaration of competing interest

The authors declare that they have no known competing financial interests or personal relationships that could have appeared to influence the work reported in this paper.

Acknowledgements

Vincenzo Spallina would like to acknowledge Prof. Fausto Gallucci and the Group of Inorganic Membrane and Membrane Reactor from the Eindhoven University of Technology (The NL) for designing and manufacturing the membrane reactor used in this work. In addition to that, as a mentor and expert on membrane technology, Prof. Gallucci has inspired a generation of researchers, in particular the authors of this work. The authors would like to acknowledge the financial support from the EPSRC "Sustainable Production of ACrylic acId from reNewable waste Glycerol" project, EP/V026089/1. Prashant Pawanipagar and Yash Bansod would also like to acknowledge the Social Welfare Department, Government of Maharashtra, India.

Appendix A. Supplementary data

Supplementary data to this article can be found online at https://doi.org/10.1016/j.cej.2026.175331.

Data availability

Data will be made available on request.

References

[1] C. Bonechi, M. Consumi, A. Donati, G. Leone, A. Magnani, G. Tamasi, C. Rossi, Biomass: an overview, in: Bioenergy Syst. Futur. Prospect. Biofuels Biohydrogen, 2017, pp. 3–42, https://doi.org/10.1016/B978-0-08-101031-0.00001-6.
[2] R. Singh, A. Gaur, P. Soni, R. Jain, G. Pant, D. Kumar, G. Kumar, S.Z. M. Shamshuddin, N.M. Mubarak, M.H. Dehghani, Suhas, K. Ansari, A review of biofuels and bioenergy production as a sustainable alternative: opportunities, challenges and future perspectives, J. Environ. Health Sci. Eng. 232 (23 (2025)) (2025) 1–20, https://doi.org/10.1007/S40201-025-00946-0.
[3] Y. Bansod, B. Crabbe, L. Forster, K. Ghasemzadeh, C. D'Agostino, Evaluating the environmental impact of crude glycerol purification derived from biodiesel production: a comparative life cycle assessment study, J. Clean. Prod. 437 (2024) 140485, https://doi.org/10.1016/J.JCLEPRO.2023.140485.
[4] U.C. Abubakar, Y. Bansod, L. Forster, V. Spallina, D. Carmine, Conversion of glycerol to acrylic acid: a review of strategies, recent developments and prospects, React. Chem. Eng. 8 (2023) 1819–1838, https://doi.org/10.1039/d3re00057e.
[5] M. Rouhany, H. Montgomery, M. Rouhany, H. Montgomery, Global biodiesel production: the state of the art and impact on, Clim. Change (2019) 1–14, https://doi.org/10.1007/978-3-030-00985-4_1.
[6] A. Sandid, V. Spallina, J. Esteban, Glycerol to value-added chemicals: state of the art and advances in reaction engineering and kinetic modelling, Fuel Process. Technol. 253 (2024) 108008, https://doi.org/10.1016/J.FUPROC.2023.108008.
[7] D. Sun, Y. Yamada, S. Sato, W. Ueda, Glycerol as a potential renewable raw material for acrylic acid production, Green Chem. 19 (2017) 3186–3213, https://doi.org/10.1039/c7gc00358g.
[8] Y. Bansod, P. Pawanipagar, K. Ghasemzadeh, C. D'agostino, Environmental Sustainability Evaluation of Glycerol and Propylene-Based Pathways to Acrylic Acid Via Different Intermediates †, 2024, https://doi.org/10.1039/d4gc01329h.
[9] Y. Bansod, P. Pawanipagar, U. Abubakar, M. Hu, H. Alhassawi, K. Ghasemzadeh, L. Forster, S. Chansai, C. Hardacre, V. Spallina, C. D'Agostino, Glycerol oxidehydration to acrylic acid experimental assessment: effect of catalyst properties, reaction parameters, and bed configurations, Chem. Eng. J. 523 (2025) 167723, https://doi.org/10.1016/J.CEJ.2025.167723.
[10] C.J. Jia, Y. Liu, W. Schmidt, A.H. Lu, F. Schüth, Small-sized HZSM-5 zeolite as highly active catalyst for gas phase dehydration of glycerol to acrolein, J. Catal. 269 (2010) 71–79, https://doi.org/10.1016/J.JCAT.2009.10.017.
[11] S.T. Wu, Q.M. She, R. Tesser, M. Di Serio, C.H. Zhou, Catalytic glycerol dehydration-oxidation to acrylic acid, Catal. Rev. 62 (2020) 481–523, https://doi.org/10.1080/01614940.2020.1719611.
[12] M.Y. Ahmad, N.I. Basir, A.Z. Abdullah, A review on one-pot synthesis of acrylic acid from glycerol on bi-functional catalysts, J. Ind. Eng. Chem. 93 (2021) 216–227, https://doi.org/10.1016/J.JIEC.2020.09.026.
[13] E. Farah, L. Demianenko, K. Engvall, E. Kantarelis, Controlling the activity and selectivity of HZSM-5 catalysts in the conversion of biomass-derived oxygenates using hierarchical structures: the effect of crystalline size and intracrystalline pore dimensions on olefins selectivity and catalyst deactivati…, Top. Catal. 6617 (66 (2023)) (2023) 1310–1328, https://doi.org/10.1007/S11244-023-01833-4.
[14] J. Shan, Z. Li, Z. Chen, D. Wang, X. Zhang, Z. Ning, Y. Xue, S. Zhu, Enhancement in catalytic performance of HZSM-5 zeolite for glycerol dehydration after acidity regulation, Chem. Eng. J. 460 (2023) 141741, https://doi.org/10.1016/J.CEJ.2023.141741.
[15] X. Gao, P. Sun, J. Liao, L. Xia, Advanced characterization techniques for the coking process of zeolites: a comprehensive review, CrystEngComm 27 (2025) 3616–3642, https://doi.org/10.1039/D5CE00156K.
[16] M.M. Diallo, S. Laforge, Y. Pouilloux, J. Mijoin, Highly efficient dehydration of glycerol to acrolein over isomorphously substituted Fe-MFI zeolites, Catal. Lett. 1488 (148 (2018)) (2018) 2283–2303, https://doi.org/10.1007/S10562-018-2470-9.
[17] X.C. Jiang, C.H. Zhou, R. Tesser, M. Di Serio, D.S. Tong, J.R. Zhang, Coking of catalysts in catalytic glycerol dehydration to acrolein, Ind. Eng. Chem. Res. 57 (2018) 10736–10753, https://doi.org/10.1021/ACS.IECR.8B01776.
[18] T. Katou, D. Vitry, W. Ueda, Structure dependency of Mo-V-O-based complex oxide catalysts in the oxidations of hydrocarbons, Catal. Today 91–92 (2004) 237–240, https://doi.org/10.1016/j.cattod.2004.03.039.
[19] W. Ueda, D. Vitry, T. Katou, Crystalline MoVO based complex oxides as selective oxidation catalysts of propane, Catal. Today 99 (2005) 43–49, https://doi.org/10.1016/J.CATTOD.2004.09.022.
[20] C. Chen, N. Kosuke, T. Murayama, W. Ueda, Single-crystalline-phase Mo3VOx: an efficient catalyst for the partial oxidation of acrolein to acrylic acid, ChemCatChem 5 (2013) 2869–2873, https://doi.org/10.1002/cctc.201300268.
[21] S. Ishikawa, X. Yi, T. Murayama, W. Ueda, Catalysis field in orthorhombic Mo3VOx oxide catalyst for the selective oxidation of ethane, propane and acrolein, Catal. Today 238 (2014) 35–40, https://doi.org/10.1016/J.CATTOD.2013.12.054.
[22] W. Ueda, Establishment of crystalline complex Mo–V–oxides as selective oxidation catalysts, J. Japan Pet. Inst. 56 (2013) 122–132, https://doi.org/10.1627/JPI.56.122.
[23] S. Ishikawa, W. Ueda, Microporous crystalline Mo–V mixed oxides for selective oxidations, Cat. Sci. Technol. 6 (2016) 617–629, https://doi.org/10.1039/C5CY01435B.
[24] S. Bagheri, N. Muhd Julkapli, Mo3VOx catalyst in biomass conversion: a review in structural evolution and reaction pathways, Int. J. Hydrogen Energy 42 (2017) 2116–2126, https://doi.org/10.1016/J.IJHYDENE.2016.09.173.
[25] S. Ishikawa, D. Kobayashi, T. Konya, S. Ohmura, T. Murayama, N. Yasuda, M. Sadakane, W. Ueda, Redox treatment of orthorhombic Mo29V11O112 and relationships between crystal structure, microporosity and catalytic performance for selective oxidation of ethane, J. Phys. Chem. C 119 (2015) 7195–7206, https://doi.org/10.1021/JP512848W/SUPPL_FILE/JP512848W_SI_001.CIF.
[26] P. Kölsch, Q. Smejkal, M. Noack, R. Schäfer, J. Caro, Partial oxidation of propane to acrolein in a membrane reactor – experimental data and computer simulation, Cat. Com. 3 (2002) 465–470, https://doi.org/10.1016/S1566-7367(02)00177-2.
[27] P. Pawanipagar, K. Ghasemzadeh, C. D', A. Ab, V. Spallina, Reactor intensification on glycerol-to-acrylic acid conversion: a modelling study †, React. Chem. Eng. (2025) https://doi.org/10.1039/d4re00481g.
[28] W. Fang, Q.J. Ge, J.F. Yu, H.Y. Xu, Catalytic selective oxidation of propane to acrylic acid in a fixed-bed reactor with an O2-distributor, Ind. Eng. Chem. Res. 50 (2011) 1962–1967, https://doi.org/10.1021/IE1018386.
[29] A. Chieregato, C. Bandinelli, P. Concepción, M.D. Soriano, F. Puzzo, F. Basile, F. Cavani, J.M.L. Nieto, Structure–reactivity correlations in vanadium-containing catalysts for one-pot glycerol oxidehydration to acrylic acid, ChemSusChem 10 (2017) 234–244, https://doi.org/10.1002/CSSC.201600954;SUBPAGE:STRING:FULL.
[30] R. Liu, T. Wang, D. Cai, Y. Jin, Highly efficient production of acrylic acid by sequential dehydration and oxidation of glycerol, Ind. Eng. Chem. Res. 53 (2014) 8667–8674, https://doi.org/10.1021/IE403270K.
[31] S. Knoche, M. Heid, N. Gora, D. Ohlig, A. Drochner, C. Hess, B. Etzold, H. Vogel, Mechanistic study on the selective oxidation of acrolein to acrylic acid: identification of the rate-limiting step via perdeuterated acrolein, ChemCatChem 11 (2019) 3242–3252, https://doi.org/10.1002/cctc.201900549.
[32] T.V. Andrushkevich, L.M. Plyasova, G.G. Kuznetsova, V.M. Bondareva, T. P. Gorshkova, I.P. Olenkova, N.I. Lebedeva, Catalytic properties of the vanadium-molybdenum oxide system for acrolein oxidation, React. Kinet. Catal. Lett. 12 (1979) 463–467, https://doi.org/10.1007/BF02061755/METRICS.
[33] T. Petzold, N. Blickhan, A. Drochner, H. Vogel, The effect of water on the heterogeneously catalyzed selective oxidation of acrolein: an isotope study, ChemCatChem 6 (2014) 2053–2058, https://doi.org/10.1002/CCTC.201400099;PAGEGROUP:STRING:PUBLICATION.
[34] A. Drochner, P. Kampe, N. Menning, N. Blickhan, T. Jekewitz, H. Vogel, Acrolein oxidation to acrylic acid on Mo/V/W-mixed oxide catalysts, Chem. Eng. Technol. 37 (2014) 398–408, https://doi.org/10.1002/ceat.201300797.
[35] T. Jekewitz, N. Blickhan, S. Endres, A. Drochner, H. Vogel, The influence of water on the selective oxidation of acrolein to acrylic acid on Mo/V/W-mixed oxides, Cat. Com. 20 (2012) 25–28, https://doi.org/10.1016/J.CATCOM.2011.12.022.
[36] B. Jabbari, E. Jalilnejad, K. Ghasemzadeh, A. Iulianelli, Modeling and optimization of a membrane gas separation based bioreactor plant for biohydrogen production by CFD–RSM combined method, J. Water Process Eng. 43 (2021) 102288, https://doi.org/10.1016/J.JWPE.2021.102288.
[37] O. Alabi-Babalola, V. Thangaraj, N. Alqahtani, H. Warsahartana, M. Smith, E. Asuquo, C. D'Agostino, A. Garforth, Thermal desorption and coke deposition

studies of spent zeolite catalysts in the hydrocracking of expanded polystyrene waste, Fuel 404 (2026) 136089, https://doi.org/10.1016/J.FUEL.2025.136089.
[38] R. Schlögl, Selective oxidation: from a still immature technology to the roots of catalysis science, Top. Catal. 2016 5917 59 (2016) 1461–1476. doi:https://doi.org/10.1007/S11244-016-0684-X.
[39] P. Kampe, L. Giebeler, D. Samuelis, J. Kunert, A. Drochner, F. Haaß, A.H. Adams, J. Ott, S. Endres, G. Schimanke, T. Buhrmester, M. Martin, H. Fuess, H. Vogel, Heterogeneously catalysed partial oxidation of acrolein to acrylic acid—structure, function and dynamics of the V–Mo–W mixed oxides, Phys. Chem. Chem. Phys. 9 (2007) 3577–3589, https://doi.org/10.1039/b700098g.
[40] M. Heid, S. Knoche, N. Gora, D. Ohlig, A. Drochner, B.J.M. Etzold, H. Vogel, Dynamics of bulk oxygen in the selective oxidation of acrolein, ChemCatChem 9 (2017) 2390–2398, https://doi.org/10.1002/cctc.201700124.
[41] J.A. Dalmon, A. Cruz-López, D. Farrusseng, N. Guilhaume, E. Iojoiu, J.C. Jalibert, S. Miachon, C. Mirodatos, A. Pantazidis, M. Rebeilleau-Dassonneville, Y. Schuurman, A.C. van Veen, Oxidation in catalytic membrane reactors, Appl. Catal. Gen. 325 (2007) 198–204, https://doi.org/10.1016/J.APCATA.2007.03.024.
[42] J.O. Fernandes, T.M. Neves, E.D. da Silva, C.A. da Rosa, V.B. Mortola, Influence of reaction parameters on glycerol dehydration over HZSM-5 catalyst, React. Kinet. Mech. Catal. 132 (2021) 485–498, https://doi.org/10.1007/S11144-020-01874-W/FIGURES/8.
[43] X. Li, E. Iglesia, Support and promoter effects in the selective oxidation of ethane to acetic acid catalyzed by Mo-V-Nb oxides, Appl. Catal. Gen. 334 (2008) 339–347, https://doi.org/10.1016/j.apcata.2007.10.021.
[44] A. Witsuthammakul, T. Sooknoi, Direct conversion of glycerol to acrylic acid via integrated dehydration–oxidation bed system, Appl. Catal. Gen. 413–414 (2012) 109–116, https://doi.org/10.1016/j.apcata.2011.10.045.
[45] U. Kuerten, M. van Sint Annaland, J. Kuipers, Int. J. Chem. React. Eng. Oxygen distribution in packed bed membrane reactors for partial oxidation systems and its effect on product selectivity, (n.d.).
[46] S. Hill, F.I. P, Channeling in packed columns, Chem. Eng. Sci. 1 (1952) 247–253, https://doi.org/10.1016/0009-2509(52)87017-4.
[47] L. Zhang, X. Meng, H. Hou, D. Shi, S. Paul, Selective oxidation of propane to acrylic acid: a critical review, Cat. Sci. Technol. 15 (2025) 4898–4915, https://doi.org/10.1039/D5CY00503E.
[48] C. O'Neill, E.E. Wolf, Partial oxidation of propane to acrolein in a dual bed inert membrane reactor, Catal. Today 156 (2010) 124–131, https://doi.org/10.1016/J.CATTOD.2010.02.041.
[49] P. Morales-Pacheco, J.M. Domínguez, L. Bucio, F. Alvarez, U. Sedran, M. Falco, Synthesis of FAU(Y)- and MFI(ZSM5)-nanosized crystallites for catalytic cracking of 1,3,5-triisopropylbenzene, Catal. Today 166 (2011) 25–38, https://doi.org/10.1016/J.CATTOD.2010.07.005.
[50] W. da S. Menezes, C.P. Rodrigues, M.M.V.M. Souza, R.L. Manfro, Conversion of glycerol into renewable hydrocarbons employing platinum and iron catalysts supported on mixed zirconium and aluminum oxides, Biomass Convers. Biorefin. 1511 (15 (2024)) (2024) 17121–17137, https://doi.org/10.1007/S13399-024-06373-9.
[51] L.F. Rasteiro, L.H. Vieira, L.G. Possato, S.H. Pulcinelli, C.V. Santilli, L. Martins, Hydrothermal synthesis of Mo-V mixed oxides possessing several crystalline phases and their performance in the catalytic oxydehydration of glycerol to acrylic acid, Catal. Today 296 (2017) 10–18, https://doi.org/10.1016/J.CATTOD.2017.04.006.
[52] S. Narayanan, J.J. Vijaya, S. Sivasanker, C. Ragupathi, T.M. Sankaranarayanan, L. J. Kennedy, Hierarchical ZSM-5 catalytic performance evaluated in the selective oxidation of styrene to benzaldehyde using TBHP, J. Porous Mater. 233 (23 (2016)) (2016) 741–752, https://doi.org/10.1007/S10934-016-0129-8.
[53] Y.P. Guo, H.J. Wang, Y.J. Guo, L.H. Guo, L.F. Chu, C.X. Guo, Fabrication and characterization of hierarchical ZSM-5 zeolites by using organosilanes as additives, Chem. Eng. J. 166 (2011) 391–400, https://doi.org/10.1016/J.CEJ.2010.10.057.
[54] J.C. Groen, L.A.A. Peffer, J.A. Moulijn, J. Pérez-Ramírez, On the introduction of intracrystalline mesoporosity in zeolites upon desilication in alkaline medium, Microporous Mesoporous Mater. 69 (2004) 29–34, https://doi.org/10.1016/J.MICROMESO.2004.01.002.
[55] P. Botella, B. Solsona, A. Martinez-Arias, J.M. López Nieto, Selective oxidation of propane to acrylic acid on MoVNbTe mixed oxides catalysts prepared by hydrothermal synthesis, Catal. Lett. 74 (2001) 149–154, https://doi.org/10.1023/A:1016614132694.
[56] P. Botella, P. Concepción, J.M. López Nieto, B. Solsona, Effect of potassium doping on the catalytic behavior of Mo-V-Sb mixed oxide catalysts in the oxidation of propane to acrylic acid, Catal. Lett. 89 (2003) 249–253, https://doi.org/10.1023/A:1025714831787/METRICS.
[57] S. Ishikawa, T. Murayama, S. Ohmura, M. Sadakane, W. Ueda, Synthesis of novel orthorhombic Mo and V based complex oxides coordinating alkylammonium cation in its heptagonal channel and their application as a catalyst, Chem. Mater. 25 (2013) 2211–2219, https://doi.org/10.1021/CM400239C.